INTEGRATED SMALL MODULAR MOLTEN SALT REACTORS AND PRE-COMPRESSION SUPERCRITICAL CARBON DIOXIDE BRAYTON CYCLE FOR SHIP PROPULSION: PRELIMINARY SYSTEM PERFORMANCE ANALYSIS AND OPTIMIZATION

Guobin Jia[1], Yang Zou[1, 2, 3*], Ye Dai[1, 2, 3], Jian Tian[1, 2], Heng Lu[1], Xiaofeng Yuan[1], Chong Zhou[1, 2, 3]

[1] Shanghai Institute of Applied Physics, Chinese Academy of Sciences, Shanghai 201800, China;
[2]University of Chinese Academy of Sciences, Beijing 100049, China
[3]National Key Laboratory of Thorium Energy, Shanghai Institute of Applied Physics, Chinese Academy of Science, Shanghai, 201800, China
** zouyang@sinap.ac.cn*

Keywords: PRE-COMPRESSION SUPERCRITICAL DIOXIDE BRAYTON CYCLE; SMALL MODULAR MOLTEN SALT REACTOR; SHIP PROPULSION; THERMODYNAMIC PERFORMANCE OPTIMIZATION

Abstract

International shipping faces stringent decarbonization mandates, necessitating zero-emission propulsion systems. This study pioneers the integration of small modular molten salt reactors with pre-compression supercritical carbon dioxide (sCO_2) Brayton cycles for zero-emission ship propulsion. Thermodynamic modeling demonstrates that the pre-compression configuration designed in this study can achieve 36.6% thermal efficiency at 640°C turbine inlet temperature while exhibiting critical operational advantages: 1) Enhanced stability against seawater temperature fluctuations (33–45°C), showing only 3.7% efficiency variation vs. 11.5% in recompression cycles. 2) Mitigated thermal stress of main heat exchanger via reduced the main compressor discharge pressure to 20 MPa. 3）Robust cold-side temperature control at the molten salt-sCO_2 heat exchanger inlet (variation <0.3%), preventing molten salt solidification below 454°C. These results resolve key maritime constraints—compactness, dynamic cold-sink resilience, and safety—establishing nuclear-powered propulsion as a technically viable pathway toward International Maritime Organization's 2050 decarbonization targets.

1 Introduction

International shipping plays a vital role in global trade but contributes significantly to greenhouse gas emissions and air pollution. Specifically, contemporary container shipping predominantly relies on Very Low Sulphur Fuel Oil (VLSFO) due to established infrastructure and lower capital costs [1]. However, VLSFO combustion generates significant greenhouse gases (2.6–3.2 Mt CO_2/year per large vessel) and air pollutants, such as SOx, NOx, PM [2-4], necessitating costly emission abatement systems. Stringent environmental regulations imposed by the International Maritime Organization (IMO), including targets for at least a 50% reduction in greenhouse gas emissions by 2050 compared to 2008 levels [5, 6], necessitate a radical transformation in marine propulsion technologies. While short-term solutions focus on efficiency improvements and alternative fuels like Liquefied Natural Gas (LNG) or biofuels, deep decarbonization requires zero-emission primary energy sources. Nuclear propulsion offers a compelling long-term pathway, providing high energy density, zero operational emissions, and potential for extended operational ranges without refueling – attributes highly advantageous for long-haul shipping routes typical of large container vessels.

Modern Ultra Large Container Vessels (ULCVs) can exceed 200,000 Deadweight Tonnage and require propulsion power upwards of 80 MW [7]. Energy demands of ULCV are characterized by continuous high-power operation for extended periods, moderate load variations due to weather and speed changes, and critical redundancy requirements. Furthermore, stringent spatial constraints within the vessel hull demand compact power generation systems with high power density. Operational reliability and safety are paramount due to the high value of cargo and the sensitive marine environment [8]. Addressing these specific requirements necessitates power systems that are efficient, compact, inherently safe, and capable of stable operation under variable loads. Small modular molten salt reactors (smMSRs) [9-11], characterized by inherent safety and high-temperature output (500-700°C), present a promising energy source for marine applications. However, conventional steam Rankine cycles face limitations in efficiency (typically <33%) and spatial footprint when integrated with PWRs [12]. In addition, container ships traversing broad geographic latitudes face

dynamic seawater temperatures (4–30°C) and flow velocities [13], significantly impacting the cold sink performance of sCO_2 cycles. Therefore, it is necessary to consider the impact of precooler outlet temperature changes on system performance.

Supercritical carbon dioxide (sCO_2) Brayton cycles, particularly recompression configurations [14], emerge as a research hotspot. Lee [10] conclude that an optimized recompression sCO_2 Brayton cycle achieves a high thermal efficiency of 47.78% for ship propulsion coupled to a small modular molten salt reactor. This represents a significant ~12% efficiency gain over traditional steam Rankine cycles. Compared to recompression [15] and intercooled cycles [16], pre-compression layouts [17] can achieve stable thermodynamic efficiency with simplified and compact architecture, making them ideal for space-constrained marine systems. Marine environments impose challenges such as temperature of cold sink fluctuations and limited space [18, 19]. Reference [20] demonstrates SMRs (molten salt or lead-bismuth cooled) enable zero-emission ship propulsion. The steam Rankine cycle achieves 35.7% efficiency, outperforming traditional systems. Reference [21] confirms nuclear propulsion's technical feasibility for zero-emission merchant shipping but identifies critical implementation barriers, which are high life-cycle costs, restrictive port or canal access due to safety concerns, and unresolved public acceptance issues remain significant hurdles for commercial adoption despite its potential for high-speed, high-value cargo transport.

Pre-compression cycles exhibit superior resilience: (1) Compared to recompression, the elimination of redundant splitter and collector in pre-compression cycles can reduces system volume effectively. (2) The pre-compression can reduce net power fluctuations under thermal source and cold source temperature variations, outperforming recompression cycles. The increasing demand for compact and high-efficiency power systems in maritime propulsion and distributed energy scenarios has driven the exploration of advanced thermodynamic cycles. This study bridges the gap between theoretical advancements in sCO_2 pre-compression cycles and real-world marine energy demands, providing a roadmap for next-generation nuclear-powered ships. The remainder of this paper is organized as follows: section 2 provides a comprehensive description of the system under investigation. Section 3 presents the system modeling approach and verification results. Section 4 reports and discusses the obtained results, analyzing their implications and validity in relation to the proposed model and existing knowledge. Finally, section 5 concludes the study by summarizing the principal findings.

2. System Description

The integrated small modular molten salt reactor (smMSR) and supercritical carbon dioxide (sCO_2) Brayton cycle system comprises three primary subsystems, as shown in Figure 1. (1) the nuclear heat source (smMSR), (2) the sCO_2 power conversion cycle, and (3) the filtered seawater cooling system. The MSR operates at 700–750°C, transferring heat via an intermediate molten salt loop to the sCO_2 cycle through a high-temperature heat exchanger. The sCO_2 cycle employs a pre-compression configuration to enhance stability under heat source and cold sink temperature fluctuations. Key components include a turbine, main compressor (MC), pre-compressor (PC), recuperators (high-temperature recuperator, HTR; low-temperature recuperator, LTR), and a seawater-cooled precooler. The pre-compression cycle splits the compression process into two stages: pre-compressor (PC) and main compressor (MC). This design decouples the MC inlet parameters from critical point of sCO_2. Figure 2 shows the T-s diagram of the pre-compression cycle under the conditions of 33 ℃ and 45 ℃ outlet temperatures of the pre cooler. Table 1 shows the overall parameters of the system.

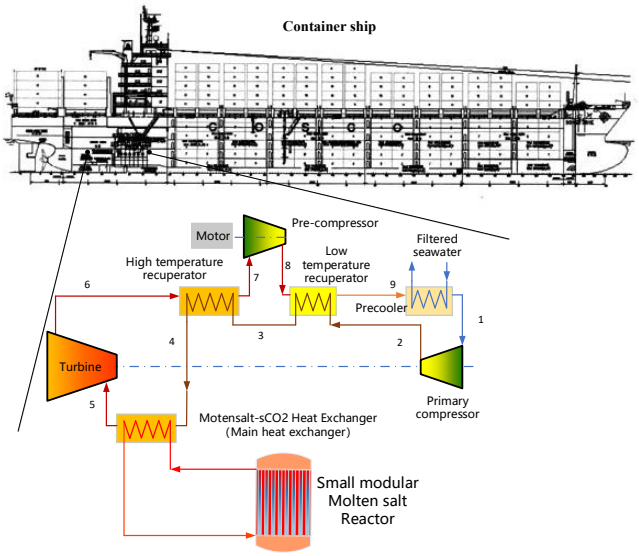

Fig. 1 Schematic diagram of the integrated smMSR – precompression sCO_2 cycle system in container ship

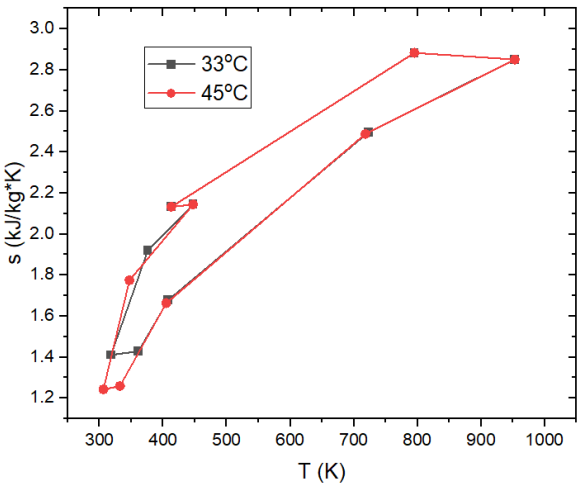

Fig. 2 T-s diagram of the sCO_2 pre-compression cycle

Table 1. Key system parameters

Parameter	Value	Unit
Thermal power of the core	100	MW

outlet Temperature of Precooler	33~45	℃
outlet pressure of the primary compressor	16~30	MPa
Inlet pressure of the Pre-compressor	8	MPa
Inlet Temperature of the Pre-compressor	140~180	℃
Outlet pressure of the Pre-compressor	9~11	MPa
Temperature end difference of LTR	15	℃
Pressure loss coefficient of main heat exchanger in hot side [22]	0.978	-
Pressure loss coefficient of high temperature recuperator in hot side [23]	0.978	-
Pressure loss coefficient of hot temperature recuperator in cold side [23]	0.985	-
Pressure loss coefficient of low temperature recuperator in hot side [23]	0.978	--
Pressure loss coefficient of cold temperature recuperator in cold side [23]	0.985	-
Pressure loss coefficient of precooler [23]	0.99	-
Isotropic efficiency of compressor [24]	82%	-
Isotropic efficiency of turbine [24]	88%	-

3 Methodology

3.1 Thermodynamic model

This study employs an in-house code to model the pre-compression sCO_2 Brayton cycle to incorporate thermodynamic governing equations. Boundary conditions are specified as fixed temperature values at the precooler outlet temperature and the main heat exchanger (MHX) cold-side. The thermodynamic analysis presented herein rests on the following established modeling foundations.

(1) The model presumes stable operational conditions.
(2) Compression and expansion operations in the compressors and turbine treated as adiabatic processes, their intrinsic inefficiency is captured using specified isentropic efficiencies. This explicitly accounts for the irreversible entropy generation inherent in real turbomachinery, differentiating it from idealized isentropic behavior.
(3) To facilitate efficient computation, pressure drop within the heat exchangers, including molten salt-sCO_2 heat exchanger, HTR, LTR and precooler, is modeled as having a proportional dependence on the inlet pressure. The magnitude of this drop is determined by conventional relative pressure loss coefficients.
(4) The thermophysical properties (e.g., density, enthalpy, entropy, specific heat capacity) of supercritical carbon dioxide are sourced from the open-source CoolProp thermophysical property database [25].

Compressors and the turbine are simulated incorporating isentropic efficiency, a standard method for characterizing real-fluid deviations from ideal adiabatic compression/expansion processes as Eq. (1) and Eq. (2) [26, 27].

$$\eta_{compressor} = \frac{h_{out,isen} - h_{in}}{h_{out,actual} - h_{in}} \quad (1)$$

$$\eta_{turbine} = \frac{h_{in} - h_{out,actual}}{h_{in} - h_{out,isen}} \quad (2)$$

where $h_{out,isen}$ denotes the enthalpy of the outlet under the same entropy condition, h_{in} represents the enthalpy of the inlet, and $h_{out,actual}$ represents the enthalpy of the outlet considering efficiency loss.

3.2 Key performance metrics

Primary system performance evaluation centers on a rigorous thermodynamic metric: thermal efficiency, which is defined as the ratio of the net electrical power output to the total high-temperature thermal energy input to the cycle, expressed according to Eq. (3) [26, 28]

$$\eta_{th} = \frac{W_{net}}{Q_{heater}} = \frac{W_{turb} - W_{MC} - W_{PC}}{Q_{heater}} \quad (3)$$

where W_{net} encompassing work contributions from the turbine and consumption by both compressors. Q_{heater} specifically refers to the thermal power transferred within the main heat exchanger (MHX), sourced from the molten salt stream. This metric quantifies the system's fundamental capability to transform heat into usable power and serves as the primary indicator for comparative analysis and optimization

In addition, LiF-NaF-KF (46.5-11.5-42.0 at%) is used as the cooling salt of secondary loop, and it has the advantages of low viscosity and low cost. Therefore, a critical operational constraint necessitates monitoring the cold-Side inlet temperature of the sCO_2 entering the main heat exchanger (MHX). This parameter is paramount for preventing salt solidification below its freezing point. The cold-side inlet temperature at the primary heat exchanger must exceed the solidus temperature (454 ℃).

3.3 Validation

The thermal efficiency analysis follows a systematic computational algorithm, depicted in Figure 3, incorporating iterative refinement to satisfy thermodynamic constraints. The sequence proceeds as follows: 1) Input fixed pressure boundary conditions, including system inlet pressure and outlet pressures of key components. Apply a designated pressure loss coefficient to determine the internal pressure distribution across the system components. 2) Using the established pressure distribution and component characteristics, calculate the Outlet temperature of the pre-compressor and Outlet temperature of the main compressor; 3) Calculate the expansion ratio across the turbine, defined as the

ratio of inlet pressure to outlet pressure and Outlet temperature of the turbine; 4) Calculate the thermal efficiency using the derived outlet temperatures, pressures, and expansion ratio. 5) Verify whether the cold side of inlet molten salt-sCO2 heat exchanger temperature remains above the freezing point of molten salt. If true, proceed to finalize the solution; If false (No), update the boundary conditions and calculate.

To validate the accuracy of the developed model, benchmark data from Sandia National Laboratories' supercritical CO_2 Brayton cycle was utilized [29]. The comparison results are in Table 2. Close agreement between the computational and empirical profiles demonstrates the validity of the proposed Brayton cycle system analysis model.

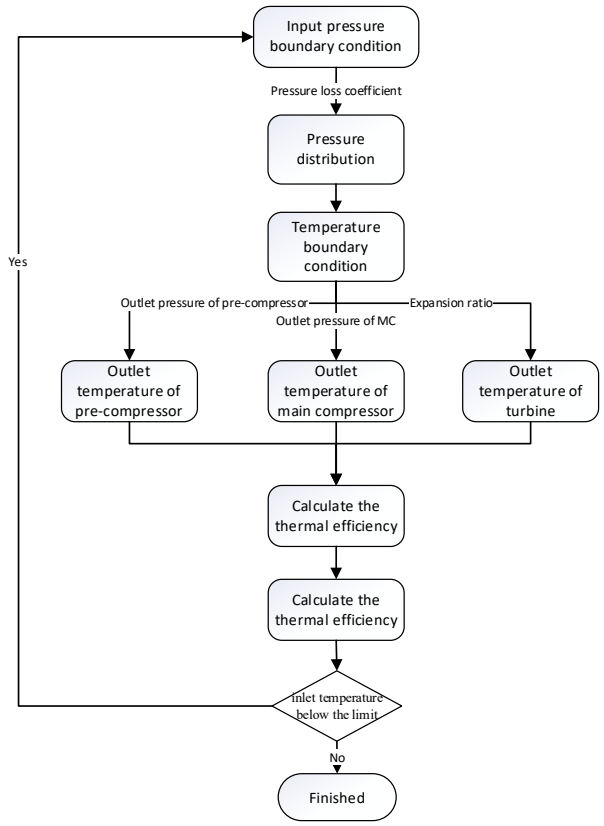

Fig. 3 Schematic diagram of system analysis

Table 2. Comparison between Sandia results and calculated results

Parameter	Sandia results	Calculated results
Turbine power (MW)	388	371.86
Primary compressor power (MW)	56.3	60.34
Re-compressor power (MW)	45.89	39.86
Heat exchanger power of low temperature recuperator (MW)	375	370.89
Heat exchanger power of high temperature recuperator (MW)	1452.4	1450.57
Power of precooler (MW)	315.5	328.34

4 Results and Discussion

4.1 The influence of precooler's outlet temperature and turbine's inlet temperature

This section analyzed the impact of turbine inlet temperature changes on system performance due to power regulation in the molten salt reactor, as well as the impact of main compressor inlet temperature changes on system performance due to seawater temperature changes.

4.1.1 Thermal efficiency: Under constant conditions including a fixed pre-compressor outlet pressure of 11 MPa and a turbine input temperature ranging from 560°C to 680°C at 24 MPa, thermal efficiency variations with precooler outlet temperature and pre-compressor inlet temperature are presented in Figure 4. The results demonstrate that thermal efficiency decreases with increasing precooler outlet temperature, primarily because the higher precooler outlet temperatures, the more main compressor power consumption, thereby reducing net power output, as shown in Figure 4. Similarly, thermal efficiency decreases with higher pre-compressor inlet temperatures, as this increases pre-compressor power consumption and reduces net system output as shown in Figure 5. Furthermore, Figure 5 reveals that pre-compressor power consumption exhibits a non-monotonic response to rising precooler temperature, initially increasing then decreasing; this occurs because increasing precooler temperature first causes a slight decrease followed by an increase in the main heat exchanger inlet enthalpy on the cold side, leading to a consequent initial decrease and subsequent increase in system mass flow rate given a constant outlet enthalpy.

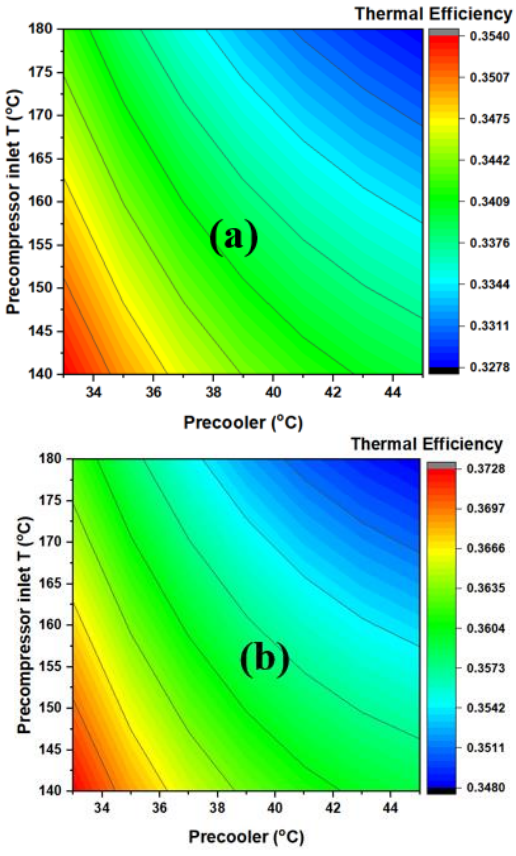

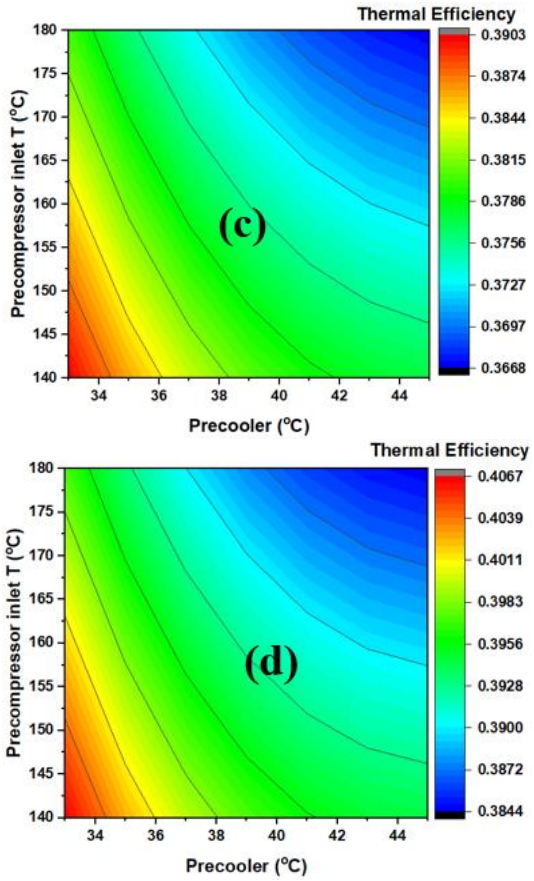

Fig. 4 The Influence of outlet temperature precooler and inlet temperature pre-compressor on Thermal Efficiency when the turbine input temperature is at 560 °C (a); turbine input temperature is at 600 °C (b); turbine input temperature is at 640 °C (c); turbine input temperature is at 680 °C (d).

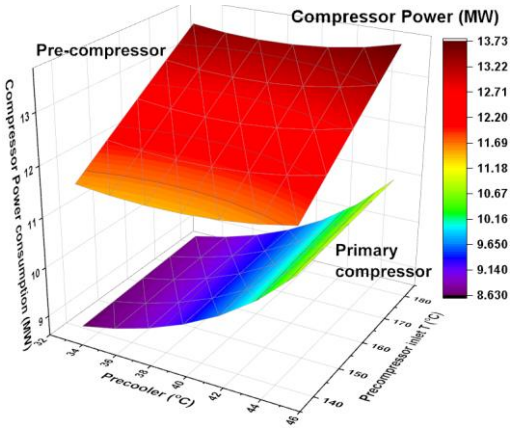

Fig. 5 The Influence of outlet temperature precooler and inlet temperature pre-compressor on compressor power and turbine power

4.1.2 Cold side of inlet temperature of the molten salt-sCO_2 heat exchanger: This section investigates the impact of turbine inlet and precooler outlet temperatures on the cold-side inlet temperature of the molten salt-sCO_2 heat exchanger, which must exceed the melting point of molten salt (454 °C).

As presented in Figure 6, the analysis reveals several key relationships. 1) the cold-side inlet temperature exhibits a minimum around 37-38°C with increasing precooler temperature. This non-monotonic behavior stems from: as precooler temperature rises, the main compressor outlet temperature and enthalpy (H_2) increase. Given constant terminal temperature difference constraints, the low-temperature recuperator hot-side outlet enthalpy (H_9) consequently increases, while its hot-side inlet enthalpy (H_8) remains unchanged due to fixed precooler inlet pressure and temperature, resulting in a decreased enthalpy difference (H_8-H_9). Through energy conservation ($H_3 = H_2 + [H_8-H_9]$), the low-temperature recuperator cold-side outlet enthalpy (H_3) decreases initially when the rate of (H_8-H_9) reduction exceeds the H_2 increase as shown in Figure 7, before subsequently rising when this relationship reverses, ultimately causing the observed minimum in molten salt heat exchanger inlet temperature. 2) higher pre-compressor inlet temperatures increase the cold-side inlet temperature due to elevated pre-compressor outlet enthalpy. Under constant precooler outlet temperature (which is also the inlet temperature of main compressor) and maximum pressure conditions, the unchanged main compressor outlet enthalpy maintains a constant low-temperature recuperator hot-side outlet enthalpy, while the enthalpy difference across its cold side expands. Energy conservation dictates a corresponding increase in the low-temperature recuperator cold-side outlet enthalpy. Although the high-temperature recuperator enthalpy difference decreases with higher pre-compressor inlet temperatures, this reduction is smaller than the enthalpy increases at the recuperator cold-side inlet, resulting in a gradual temperature rise at the molten salt-sCO_2 heat exchanger inlet.

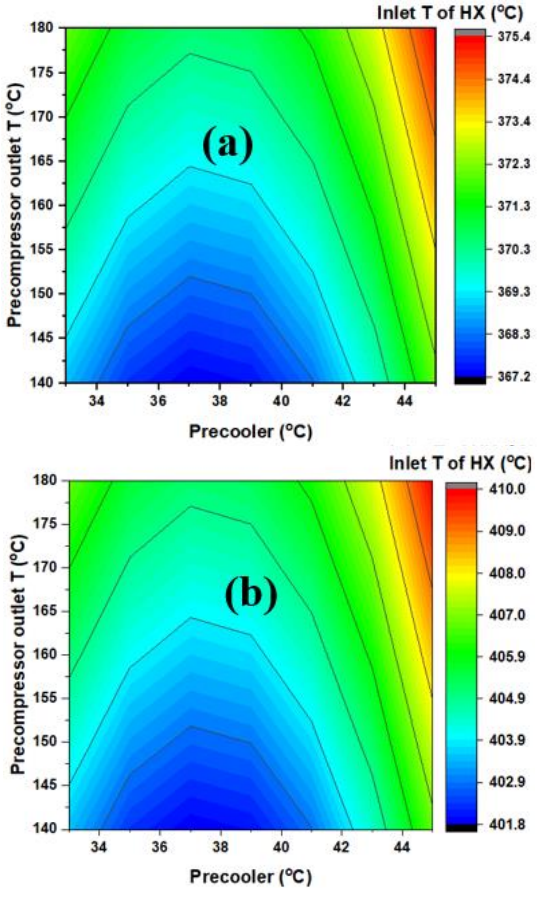

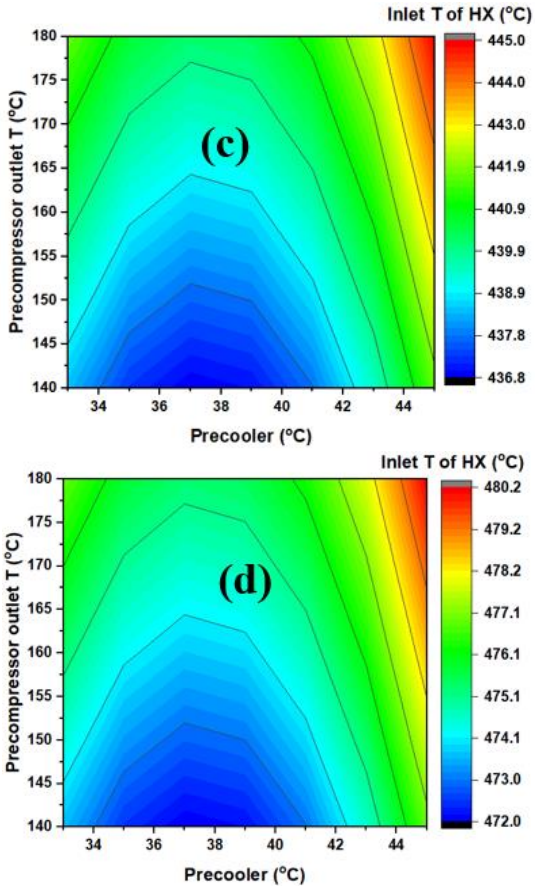

Fig. 6 The Influence of outlet temperature precooler and inlet temperature pre-compressor on cold side of inlet temperature of the molten salt-sCO_2 heat exchanger when the turbine input temperature is at 560 °C (a); turbine input temperature is at 600 °C (b); turbine input temperature is at 640 °C (c); turbine input temperature is at 680 °C (d).

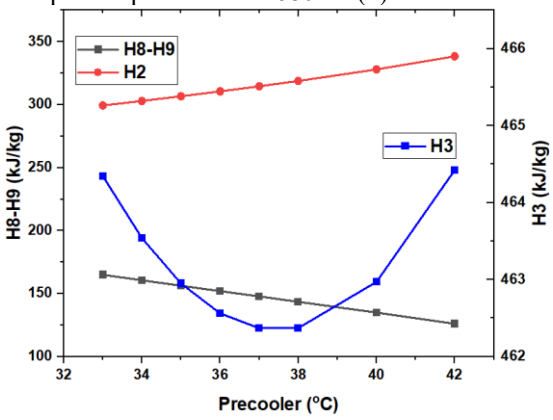

Fig. 7 The Influence of precooler's outlet temperature on system enthalpy

4.2 The influence of outlet pressure of pre-compressor and main compressor

4.2.1 Thermal efficiency: This section examines the influence of pre-compressor outlet pressure and system maximum pressure (main compressor outlet pressure) on system performance. Figure 8 present the thermal efficiency variations across the investigated pre-compressor outlet pressure range of 9–11 MPa for turbine inlet temperature of 560°C, 600°C, 640°C, and 680°C. Key findings emerge: (1) Thermal efficiency consistently increases with higher system maximum pressure. This improvement occurs despite increased main compressor work consumption (Figure 9a), because the resultant enhancement in turbine power output (Figure 9b) exceeds the additional compression work required below approximately 30 MPa. (2) Optimal efficiency initially occurs at the minimum pre-compressor outlet pressure (9 MPa) for system maximum pressures up to 22 MPa. However, when pressures exceeding 22 MPa, the maximum thermal efficiency shifts to the highest pre-compressor outlet pressure (11 MPa). This transition arises because the pre-compressor consumes more work than the main compressor below 22 MPa. As the system pressure increases beyond this point, the work ratio reverses (main compressor exceeds pre-compressor), simultaneously triggering a substantial increase in turbine output that outweighs the combined growth in compressor power consumption.

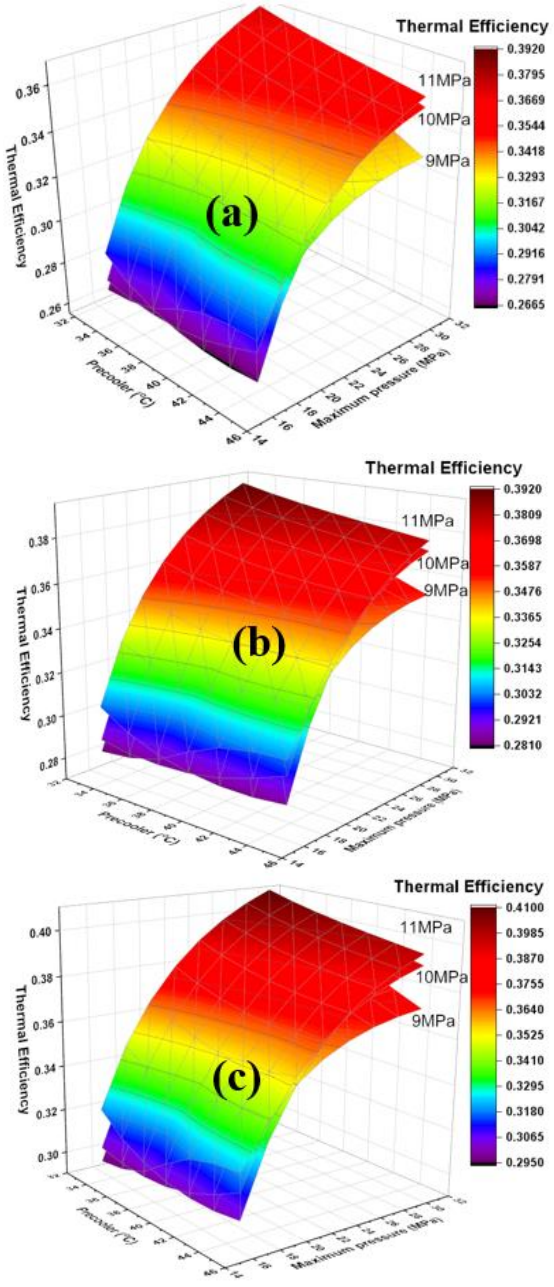

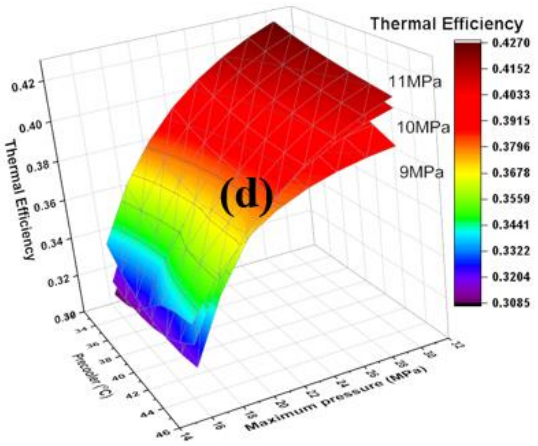

Fig. 8 The Influence of outlet temperature precooler, maximum pressure and outlet pressure of pre-compressor on thermal efficiency when the turbine input temperature is at 560 °C (a); turbine input temperature is at 600 °C (b); turbine input temperature is at 640 °C (c); turbine input temperature is at 680 °C (d).

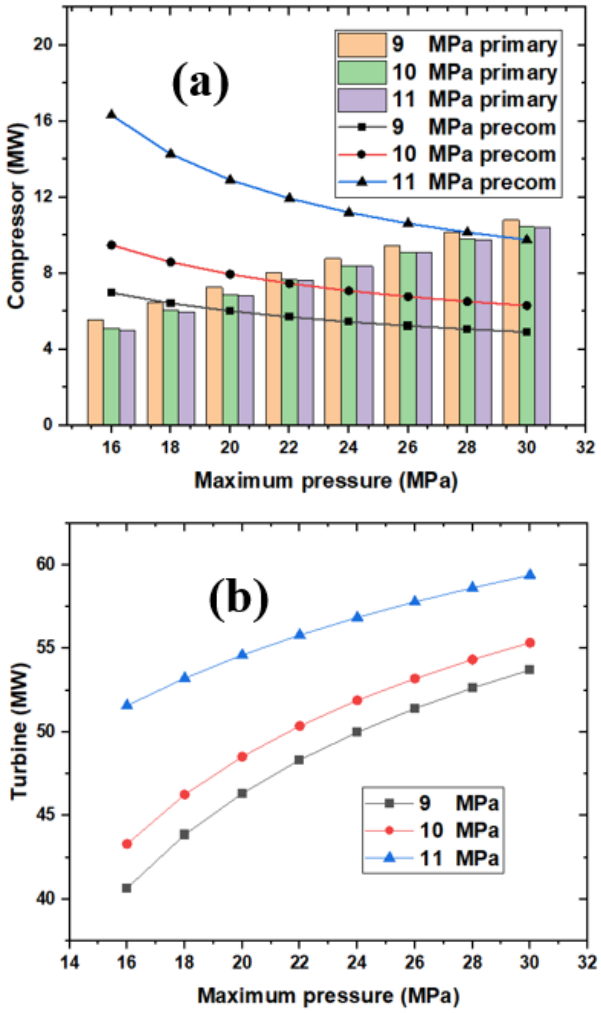

Fig. 9 The Influence of maximum pressure and outlet pressure of pre-compressor on compressor work (a) and turbine work (b)

4.2.2 Code side inlet temperature of the molten salt-sCO₂ heat exchanger: The variation of the cold-side inlet temperature in the molten salt - sCO₂ heat exchanger with precooler outlet temperature, pre-compressor outlet pressure, and system maximum pressure is presented in Figure 10. The results reveal two principal trends: (1) Precooler outlet temperature exhibits minimal influence on the primary heater inlet temperature at pre-compressor outlet pressures of 10 MPa and 11 MPa. However, at 9 MPa, the inlet temperature increases markedly when precooler outlet temperatures exceed 39°C. This heightened sensitivity stems from the main compressor inlet conditions operating near the critical point at 9 MPa, where sCO₂ undergoes significant thermophysical property variations. Specifically, as shown in Figure 11, enthalpy experiences a substantial increase beyond 39°C due to these nonlinear property changes, directly elevating the enthalpy and consequently the temperature at the molten salt heat exchanger inlet. (2) Increasing system maximum pressure (main compressor outlet pressure) induces a monotonic decrease in the heat exchanger cold-side inlet temperature. This inverse relationship arises because higher pressures increase the enthalpy difference across the cold side of the heat exchanger. With the hot-side outlet temperature constrained under constant terminal temperature difference conditions, the cold-side inlet temperature necessarily decreases to accommodate the larger enthalpy change.

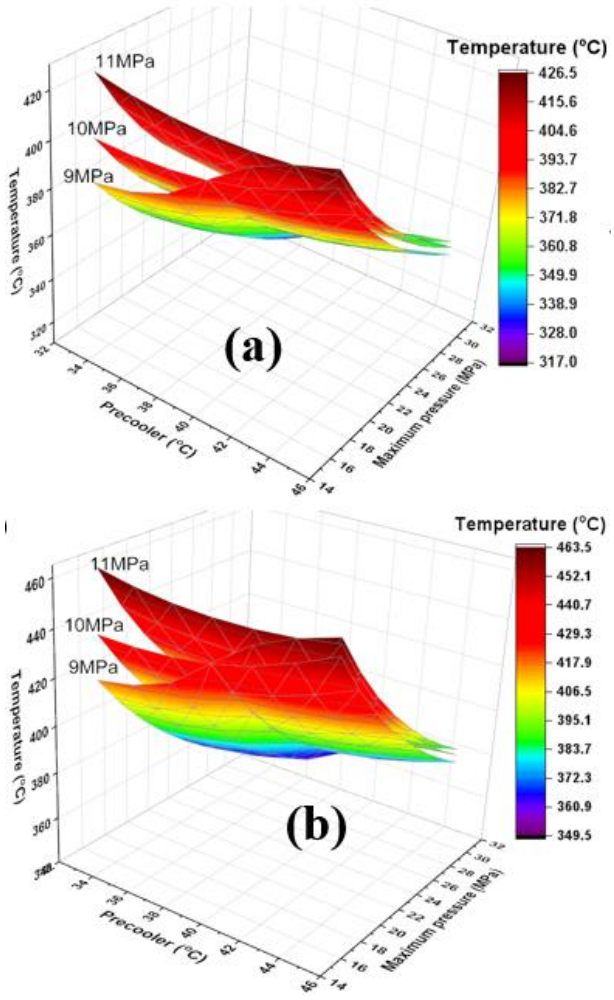

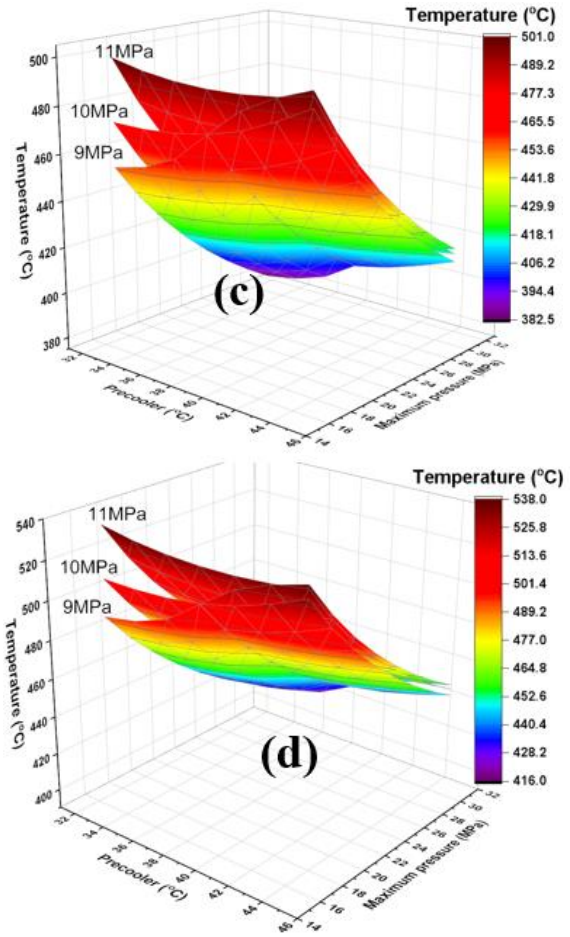

Fig. 10 The Influence of outlet temperature precooler, maximum pressure and outlet pressure of pre-compressor on cold side of inlet temperature of the molten salt-sCO_2 heat exchanger when the turbine and pre-compressor input temperature is at 560 °C and 140 °C, respectively; (a); turbine and pre-compressor input temperature is at 600 °C and 140 °C, respectively; (b); turbine and pre-compressor input temperature is at 640 °C and 140 °C, respectively; (c); turbine and pre-compressor input temperature is at 680 °C and 140 °C, respectively (d).

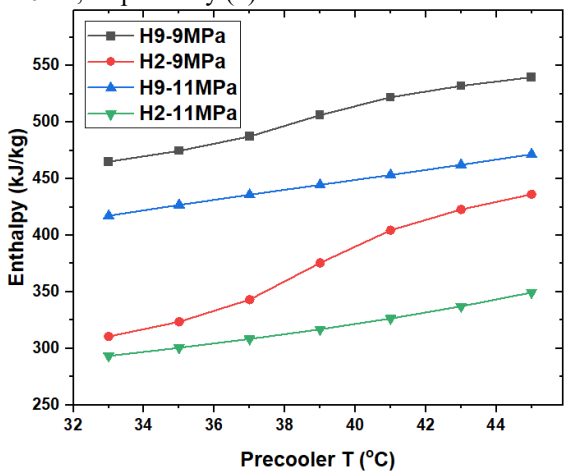

Fig. 11 The Influence of outlet temperature of precooler and outlet pressure of pre-compressor on

4.3 Optimized system parameters

The optimized sCO_2 precompression cycle integrated with the molten salt reactor system parameters are interpreted as Figure 12. The finalized sCO_2 power cycle achieves a thermal efficiency of 36.6%, operating with a molten salt heat source entering the primary Molten Salt-sCO_2 Heat Exchanger at 640°C . Within this exchanger, the sCO_2 working fluid is heated to 640°C and pressurized to 19.0 MPa before expansion through the turbine. The turbine exhausts sCO_2 at 534.7°C and 8.2MPa , feeding into the High-Temperature Recuperator (HTR), and the heat exchange power is 208.8 MW, which cools the stream to 140°C at 8.0 MPa. Subsequent compressing to 174.3 at 11MPa via pre-compressor, heat recovery occurs in the low-temperature recuperator (LTR), and the heat exchange power is 82.5 MW, which lowers the temperature further to 62.1°C at 10.8 MPa. After rejection 63.4 MW of heat in the Precooler to achieve a near-critical condition of 33.0°C at 10.65 MPa. the main compressor elevates pressure to 20 MPa with an outlet temperature of 47.1 °C. The compressed sCO_2 is then preheated sequentially in the LTR to 121.3 °C at 19.7 MPa and in the HTR to 464.0°C at 19.4 MPa before returning to the primary heat exchanger, completing the cycle. This configuration demonstrates effective thermal integration and strict adherence to engineering constraints while achieving the reported efficiency.

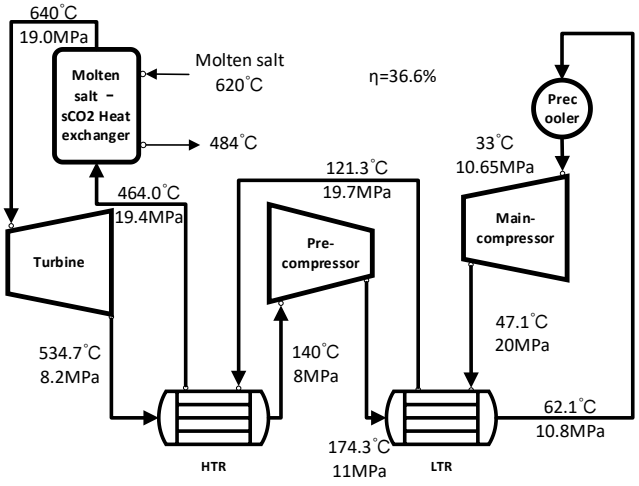

Fig. 12 Schematic diagram of optimized system parameters

A comparative assessment of two sCO_2 thermodynamic cycles—recompression cycle (RCC) and pre-compression cycle (PRC)—was conducted at fixed turbine inlet temperature (640°C) and main compressor outlet pressure (20 MPa) to evaluate thermal efficiency and inlet temperature of main heat exchanger in cold side sensitivity to precooler outlet temperature variations, as illustrated in Figure 13. The analysis reveals two critical findings: 1) Regarding the thermal efficiency, the PRC configuration exhibits markedly lower sensitivity (3.7%) to precooler outlet temperature fluctuations (33~45°C) compared to the RCC (11.5%), which demonstrates the most pronounced efficiency variations. This stability arises because the PRC cycle's main compressor inlet operates sufficiently distant from the critical point of CO_2, thereby

minimizing property-induced thermodynamic anomalies. 2) The recompression cycle demonstrates a significantly higher inlet temperature (~494°C) at the main heat exchanger cold-side compared to the pre-compression configuration, but PRC exhibits exceptionally stable thermal behavior with minimal variation across the precooler temperature range.

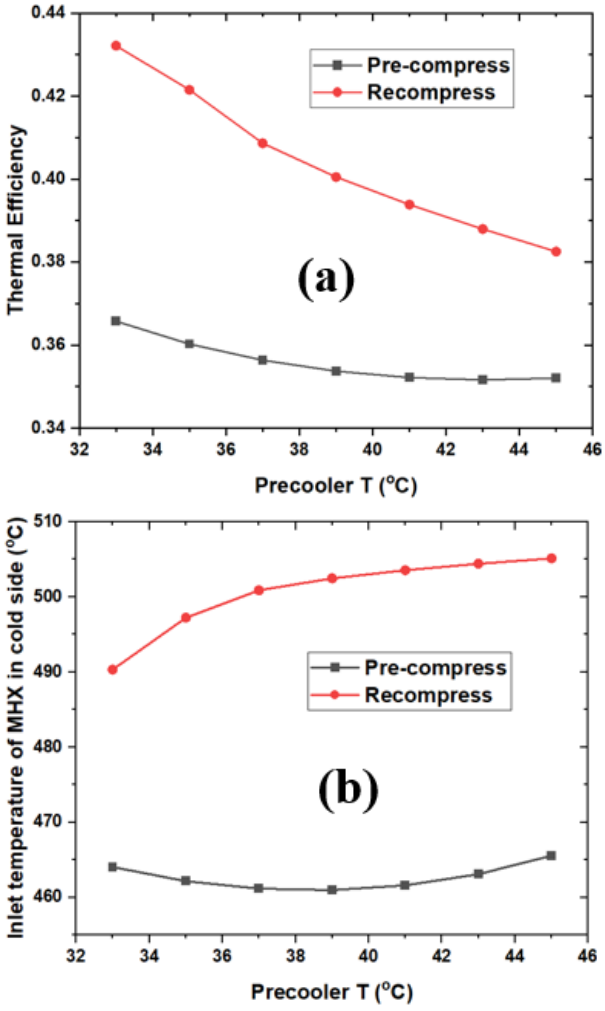

Fig. 13 Comparison of thermal efficiency (a) and inlet temperature of main heat exchanger in cold sid (b) between split flow recompression and precompression cycle

5 Conclusions

This study addresses a critical gap in marine nuclear power system design by pioneering an integrated analysis of molten salt reactor (MSR) and supercritical CO_2 power cycles under marine operational constraint. Three key advances emerge:

1) The integrated MSR and sCO_2 pre-compression cycle designed in this study exhibits inherent stability against seawater temperature perturbations—a decisive advantage over recompression cycles. This stems from strategically decoupling the main compressor inlet from critical-point property variations.
2) Implementation of a ≤20 MPa main compressor discharge pressure effectively mitigates thermal stress risks in the primary heat exchanger while maintaining 36.6% efficiency.
3) The pre-compression cycle designed in this study exhibits markedly lower sensitivity in thermal efficiency (3.7% vs 11.5%) and inlet temperature at the main heat exchanger cold-side (0.3% vs 3%) compared to recompression cycle.

These innovations position nuclear-powered shipping as a technically viable pathway to IMO's 2050 emission targets. Future work will quantify transient performance under wave-induced motion and implement dynamic control strategies for load-following operations.

6 Acknowledgements

This research was funded by the Physical Study on Heat Transfer of Heat Pipe Micro Molten Salt Reactor System (Grant No. E541220101) and the Research and verification of multi physics coupling effects based on 2MW liquid fuel thorium based molten salt experimental reactor (Grant No. E455960301).

7 References

[1] Wu, P.C. and C.Y. Lin, *Cost-Benefit Evaluation on Promising Strategies in Compliance with Low Sulfur Policy of IMO.* JOURNAL OF MARINE SCIENCE AND ENGINEERING, 2021. 9(1).
[2] Dong, X., et al., *Environmental and health impacts of reduced PM2.5 and trace metals from ship emissions under low-sulfur fuel oil policy in Shanghai, China.* Environmental Pollution, 2025. 377: p. 126409.
[3] Shi, J., et al., *The impact of low-sulfur marine fuel policy on air pollution in global coastal cities.* Sustainable Horizons, 2025. 14: p. 100130.
[4] Anastasopolos, A.T., et al., *Evaluating the effectiveness of low-sulphur marine fuel regulations at improving urban ambient PM2.5 air quality: Source apportionment of PM2.5 at Canadian Atlantic and Pacific coast cities with implementation of the North American Emissions Control Area.* Science of The Total Environment, 2023. 904: p. 166965.
[5] Bilgili, L. and A.I. Ölçer, *IMO 2023 strategy-Where are we and what's next?* Marine Policy, 2024. 160: p. 105953.
[6] Song, S.-K., et al., *Impact of international Maritime Organization 2020 sulfur content regulations on port air quality at international hub port.* Journal of Cleaner Production, 2022. 347: p. 131298.
[7] Wang, J., et al., *Dimensional precision controlling on out-of-plane welding distortion of major structures in fabrication of ultra large container ship with 20000TEU.* Ocean Engineering, 2020. 199: p. 106993.
[8] Nguyen, S., C.P. Shu-Ling, and Y. and Du, *Container shipping operational risks: an overview of assessment and analysis.* Maritime Policy & Management, 2022. 49(2): p. 279–299.
[9] Huang, J.-L., et al., *Dynamic simulation analysis of molten salt reactor-coupled air–steam combined cycle power generation system.* Nuclear Science and Techniques, 2024. 35(2): p. 30.
[10] Lee, W., et al., *Design considerations of the supercritical carbon dioxide Brayton cycle of small modular molten salt reactor for ship propulsion.* Progress in Nuclear

Energy, 2023. 163: p. 104835.
[11] Guo, Y., et al., *Coupling a small modular molten salt reactor with desalination.* Nuclear Engineering and Design, 2023. 413: p. 112513.
[12] Wang, C., et al., *Parametric optimization of steam cycle in PWR nuclear power plant using improved genetic-simplex algorithm.* Applied Thermal Engineering, 2017. 125: p. 830–845.
[13] Dipper, F., *Chapter 2 - The seawater environment and ecological adaptations*, in *Elements of Marine Ecology (Fifth Edition)*, F. Dipper, Editor. 2022, Butterworth-Heinemann. p. 37–151.
[14] Crespi, F., et al., *Supercritical carbon dioxide cycles for power generation: A review.* Applied Energy, 2017. 195: p. 152–183.
[15] Reznicek, E.P., T. Neises, and R.J. Braun, *Optimization and techno-economic comparison of regenerators and recuperators in sCO2 recompression Brayton cycles for concentrating solar power applications.* Solar Energy, 2022. 238: p. 327–340.
[16] Jiang, J., et al., *Performance evaluation of supercritical CO2 Brayton cycle with two-stage compression and intercooling.* Case Studies in Thermal Engineering, 2024. 64: p. 105503.
[17] Abdelghafar, M.M., M.A. Hassan, and H. Kayed, *Comprehensive analysis of combined power cycles driven by sCO2-based concentrated solar power: Energy, exergy, and exergoeconomic perspectives.* Energy Conversion and Management, 2024. 301: p. 118046.
[18] Vincze, M., I.D. Borcia, and U. Harlander, *Temperature fluctuations in a changing climate: an ensemble-based experimental approach.* Scientific Reports, 2017. 7(1): p. 254.
[19] Boero, F., *Fluctuations and Variations in Coastal Marine Environments.* Marine Ecology, 1994. 15(1): p. 3–25.
[20] Hirdaris, S.E., et al., *Considerations on the potential use of Nuclear Small Modular Reactor (SMR) technology for merchant marine propulsion.* Ocean Engineering, 2014. 79: p. 101–130.
[21] Bayraktar, M. and O. Yüksel, *Analysis of the nuclear energy systems as an alternative propulsion system option on commercial marine vessels by utilizing the SWOT-AHP method.* Nuclear Engineering and Design, 2023. 407: p. 112265.
[22] Tournier, J.-M.P. and M.S. El-Genk, *Properties of noble gases and binary mixtures for closed Brayton Cycle applications.* Energy Conversion and Management, 2008. 49(3): p. 469–492.
[23] El-Genk, M.S. and J.-M. Tournier, *Noble-Gas Binary Mixtures for Closed-Brayton-Cycle Space Reactor Power Systems.* Journal of Propulsion and Power, 2007. 23(4): p. 863–873.
[24] El-Genk, M.S. and J.-M. Tournier, *Noble gas binary mixtures for gas-cooled reactor power plants.* Nuclear Engineering and Design, 2008. 238(6): p. 1353–1372.
[25] Casari, N., M. Pinelli, and A. Suman, *Analysis of CoolProp library for the assessment of uncertainty propagation for refrigerant fluids in state diagrams and thermodynamic properties.* International Journal of Refrigeration-Revue Internationale Du Froid, 2019. 107: p. 214–224.
[26] Jia, G., et al., *Thermodynamic Analysis and Optimization of Mobile Nuclear System.* Energies, 2025. 18(1): p. 113.
[27] Wang, Q., et al., *Thermodynamic analysis and optimization of the combined supercritical carbon dioxide Brayton cycle and organic Rankine cycle-based nuclear hydrogen production system.* International Journal of Energy Research, 2022. 46(2): p. 832–859.
[28] Ribeiro, G.B., F.A. Braz Filho, and L.N.F. Guimarães, *Thermodynamic analysis and optimization of a Closed Regenerative Brayton Cycle for nuclear space power systems.* Applied Thermal Engineering, 2015. 90: p. 250–257.
[29] [Wright, S., et al., *Operation and analysis of a supercritical CO2 Brayton cycle.* 2010.